LA-UR -76-2284

MASTER

TITLE: EPITAXIAL SILICON SEMICONDUCTOR DETECTORS, PAST DEVELOPMENTS, FUTURE PROSPECTS

CONF-761006--8

AUTHOR(S): C. R. Gruhn

SUBMITTED TO: 1976 Nuclear Science Symposium to be published in the IEEE Proceedings

los alamos
scientific laboratory
of the University of California
LOS ALAMOS, NEW MEXICO 87545

Form No. 836
St. No. 2629
1/75

UNITED STATES
ENERGY RESEARCH AND
DEVELOPMENT ADMINISTRATION
CONTRACT W-7405-ENG. 36

EPITAXIAL SILICON SEMICONDUCTOR DETECTORS PAST DEVELOPMENTS, FUTURE PROSPECTS†

C. R. Gruhn*

ABSTRACT

A review of the main physical characteristics of epitaxial silicon as it relates to detector development is presented. As examples of applications results are presented on (1) epitaxial silicon avalanche diodes (ESAD); signal-to-noise, non-linear aspects of the avalanche gain mechanism, gain-bandwidth product, (2) ultrathin epitaxial silicon surface barrier (ESSB) detectors, response to heavy ions, (3) an all-epitaxial silicon diode (ESD), response to heavy ions, charge transport and charge defect. Future prospects of epitaxial silicon as it relates to new detector designs are summarized.

I. INTRODUCTION

The first all epitaxial silicon semiconductor detectors[1,2] were produced in 1973. These detectors consisted of a thin n-type epitaxial layer with a Schottky barrier at the surface. The response of these detectors was studied with an alpha source. Since these first works, a number of more complex detector designs using some of the unique features that the epitaxial material allows have been investigated.[3,4,5] It is the purpose of this paper to review the performance and unique features that these detector designs exhibited.

In part II a review of those physical characteristics peculiar to the epitaxial silicon as applied in detector development is given. In part III three examples of epitaxial silicon applications are presented. A discussion of the advantages and disadvantages of the epitaxial design vs alternative designs is given. Part IV is a biased view as to the future prospects of epitaxial silicon in new detector designs.

II. SOME PHYSICAL CHARACTERISTICS OF EPITAXIAL SILICON

The epitaxial silicon growth process is a crystal growth process in which the crystal is grown upon a silicon substrate from a vapor phase containing a controlled amount of dopeant. The epitaxial growth rate is much faster than the diffusion rate of a number of dopeants. It is for this reason that layers having a uniform resistivity can be realized over the distance of tens of microns and relatively sharp boundaries. Epitaxial layers can also be grown over diffused areas with little auto doping. The process is not perfect; in some cases one can have an unwanted impurity from the substrate autodope the epitaxial layer. This problem is generally controlled by specifying the quality of substrate material. A major reason for considering epitaxial silicon as a detector material is because it is a well developed technology of the semiconductor device industry and is commercially available.

Table I lists some of the properties of commercially available epitaxial silicon.

Table I

Some Properties of Commercially Available Epitaxial Silicon

Approximate range of resistivities available in epitaxial layers (±10%)	10^{-2}- $10^{2}\Omega$cm
Boundary definition between epitaxial layers (varies); sharpest is	∿ 1-2 μm
Range of thicknesses available in epitaxial layers (±10%)	1-100 μm
Maximum diameter of epitaxial silicon wafers available	∿ 10 cm
Typical cost for single epitaxial layer on substrate (Ø - 1.5"), per wafer	∿ $15.00
Maximum number of stacked epitaxial layers attempted successfully to date	∿ 4
Crystal orientation (other orientations are possible)	2-3° off the 111 axis

This range of resistivities available lends itself to the design of thin and relatively fast diodes. Both the charge transit times and dielectric relaxation times for such diodes can be relatively short. In Table II a list of the corresponding relaxation times and maximum charge transit times for this range of resistivities is given. In addition, the maximum depletion widths and voltages are listed for a Schottky barrier diode on n-type silicon.

Because this range of resistivities is factors of 10 to 100 lower than those used in the more conventional silicon semiconductor detectors, the radiation lifetime is expected to be longer by at least the same factor. This is because the signals are realized in a shorter time and therefore are less vulnerable to radiation-induced lifetime degradation. In addition, the greater impurity densities of the epitaxial material will provide a higher threshold for problems introduced by radiation-induced defects or impurities.

Table II also indicates a compatibility between the range of depletion widths and thicknesses available in the epitaxial layers. In addition, it should be pointed out that a selective etch process has been developed[6] which allows one to remove the substrate but not the epitaxial layer. This means that the uniformity in thickness of the remaining silicon film is determined by the epitaxial growth process. Uniformity of thickness of the order of 0.1 μm can be realized for the thinnest epitaxial films.

Because of the highly developed technology in back of the production of epitaxial silicon the cost per wafer is relatively low (∿ $15.00/single epitaxial wafer) and the available areas are relatively large (∿ 75 cm^2). Other technologies standardized with the use of the epitaxial wafer exist. For example, the photolithographic and monolithic processing associated with integrated circuit production can be readily applied to detector development problems using the standardized wafers.

†Work performed under the auspices of the U.S. Energy Research and Development Administration, Contract W-7405-ENG. 36.

*University of California, Los Alamos Scientific Laboratory, P. O. Box 1663, Los Alamos, NM 87545.

Table II

Resistivity (n-type) ρ (Ω cm)	Impurity Concentration C_B (cm-3)	Depletion Width W_B (microns)	Breakdown Voltage V_B (volts)	Dielectric Relaxation time (ps)	Charge Transit Time (ps) t_t
.04	6.5×10^{17}	.1	1.0	.042	1.0
.10	10^{17}	.35	4.9	.10	3.5
.18	5×10^{16}	.6	8.0	.18	6.
.60	10^{16}	2.2	32.	.6	22.
1.0	5×10^{15}	3.5	49.	1.0	35.
4.8	10^{15}	15.	188.	4.8	150.
9.0	5×10^{14}	25.	278.	9.0	250.
55.0	10^{14}	110.	880.	110.	1100.

The fact that one can stack the epitaxial layers gives a high degree of design freedom. The impurity profile can be tailored to give a particular field distribution and therefore charge transport characteristic. The advantages of this feature are seen in the detector design examples given in Part III.

III. EXAMPLES OF APPLICATIONS OF EPITAXIAL SILICON IN DETECTOR DESIGNS

ESAD - Epitaxial Silicon Avalanche Diode[3,4]

The use of internal amplification in a semiconductor is not particularly new.[7,8,9,10,11] The motivation for including amplification within the detector has been twofold, first to improve the signal-to-noise ratio by amplifying before the noise sources, and second to give more signal with less electronics. From the viewpoint of improving the signal-to-noise ratio, the major limitation has been with the uniformity of gain across the detector.[3,10] In the case of the avalanche diode, the uniformity in gain depends upon achieving a uniform high value of the field. This has been most easily accomplished using the "reach through before avalanche" concept of Read.[12] This field stabilization concept depends upon the production of a thin layer of higher resistivity material. The three fabrication techniques thus far used for this purpose have been diffusion, ion implantation (with diffusion), and epitaxial. The latter two have been shown to give the greatest uniformity in the field.[3,10] The epitaxial technique offers somewhat more control in the creation of the field profile. This is expected to be important in future developments because the energy exchange mechanisms not only depend upon the field but also the field-length product.

Design. The design of the ESAD is shown in Fig. 1. The design establishes the p^+-p structure (necessary for the field stabilization concept of Read using a double epitaxial layer on the p^{++} substrate. A mesa (4-mm in diameter) is etched leading an island of p^+-type epitaxial material (6-μm thick) upon the second p-type epitaxial layer (30-μm thick). A phosphorous diffusion yields the n^{++} layer of 1-μm thick. The overall detector area including guard ring is defined by etching a second mesa of larger diameter than the first. The p^+ region is completely buried, thus leaving the highest field regions isolated from the surfaces.

In Fig. 2 the impurity concentration and electric field profiles are shown. The maximum field is given as a function of bias by the expression

$$E_{max} = \frac{2 N_{AO} \cdot x_0}{W_1^2} + 2\left[N_{Al}\left(V - \frac{x_0^2 \cdot N_{AO}}{W_1^2}\right)\right]^{1/2} \Big/ W_1 \qquad (1)$$

where x_0 is the width of the p^+ region

V_0 is the bias required to just deplete the p^+ region

and $x_0 = W_1 (V_0/N_{AO})^{1/2}$

where N_{AO} is the ionized impurity concentration in the p^+ region

W_1 is a temperature dependent constant

and $x_1 - x_0$ is the "reach through" distance

$$(x_1 - x_0) = W_1 ((V-V_0)/N_{Al})^{1/2}$$

where N_{Al} is the ionized impurity concentration in the p region.

It is seen that the precision and value of E_{max} is determined primarily by the areal density, $N_{AO} \cdot x_0$ of ionized impurities in the p^+ region.

E_{max} is plotted as a function of reverse bias in Fig. 3.

Gain, Uniformity, and Stability. Some insight with regard to the question of gain uniformity and stability can be obtained from the expression relating the gain, M, to the reverse bias, V, relative to the breakdown bias, V_B, for a step junction.[13]

$$M = \frac{1}{1 - (V/V_B)^2} \qquad (2)$$

In our design we have a step junction up to biases which "reach through." In terms of the electric field

$$M = \frac{1}{1 - \left(\frac{E}{E_{crit}}\right)^4} \qquad (3)$$

It is now easily seen that the uniformity in gain, M, is determined by the uniformity of the areal density of

impurities in the p^+ region, $N_{AO} \cdot x_O$. For high gain

$$\frac{\Delta M}{M} \propto 4 \cdot M \frac{\Delta(N_{AO} \cdot x_O)}{N_{AO} \cdot x_O} \tag{4}$$

This expression indicates the extreme sensitivity the uniformity of gain, $\Delta M/M$, has upon nonuniformities associated with the p^+ region. It is, in fact, for this problem that epitaxial growth methods are so promising.

In a similar fashion the dependence of the gain on small temperature changes is found from Eq. 2. Assuming a high value of gain:

$$\frac{\Delta M}{M} \quad -2 \cdot M \frac{\Delta V_B}{\Delta T} \cdot \frac{\Delta T}{V_B} \tag{5}$$

where $\frac{\Delta V_B}{\Delta T} = .1 \frac{\text{Volts}}{^\circ C}$ at $V_B = 100$ volts.

Thus for this case

$$\frac{1}{M} \cdot \frac{\Delta M}{\Delta T} = -2 \cdot M \times 10^{-3}/^\circ C \tag{6}$$

Note that the gain increases as the temperature decreases.

Gain, Nonlinearities.[4] A major cause for a nonlinearity in the gain is due to the space charge limitations of the avalanche. In the detection of the ionization of a charge particle, the space charge reduction of the field is expected to occur in some proportion of the initial density of ionization. This results in a reduction of gain and can be accounted by the modification of expression 3.[14]

$$M = \frac{1}{1 - \left(\frac{E - F_{sc}}{E_{crit}}\right)^4} \tag{7}$$

where E_{sc} is the field due to the space charge in the avalanche.

In the detection of a charge particle

$$E_{sc} \propto \left(\frac{\partial \bar{\varepsilon}}{\partial x}\right)^n \tag{8}$$

where $\partial\varepsilon/\partial x$ is the average energy loss per unit thickness. It is then easily shown that the gain, M, has the following dependence on the density of ionization:

$$M = \frac{M_o}{1 - (M_o - 1) \cdot 4a \frac{\partial \bar{\varepsilon}^n}{\partial x}} \tag{9}$$

where M_o is the gain in the limit of zero ionization

a and n are constants that depend upon the material and geometric aspects of the design.

This type of nonlinearity has been confirmed experimentally.[4] In Fig. 4 a spectrum is shown indicating the differences in gain for a broad range of densities of ionization. This spectrum was taken using the LASL tandem Van de Graaff and a beam of 15 MeV alpha particles scattering from a CH_{2N} target. The incident energies were determined from the reaction kinematics. The kinematics also helped to identify the peaks with gain and the peaks associated with the response of the guard structure (unity gain). Figure 5 shows the gain as a function of the average energy loss and assymtotic gain, M_o. The data is fit by Eq. 9. The use of the avalanche gain is most favorable for lightly ionizing particles.

X-Ray Response. Figure 6 shows the response of the ESAD to ^{55}Fe x-rays (5.9 keV). For this particular spectrum the gain in the avalanche zone was 18. A best resolution of 1.74 keV (FWHM) has been observed at this gain. The electronic contributions to the noise were measured by use of a pulser set at 13 keV times the gain. This noise was limited by the high capacitance of the thin p-type epitaxial layer (30 μm). In the design of an x-ray detector using the epitaxial technique this layer could be at least 3 times thicker. A maximum nonuniformity in gain was obtained by unfolding the electronic contribution to the noise, $\Delta M/M = 0.177$. Using Eq. 4 we see that this infers a maximum nonuniformity in the impurity areal density of 0.25%. It should also be noted that the pulse height of the pulser coincides with that expected for a minimum ionizing particle and a gain of 18. For this case we then have a S/N = 9.4 for minimum ionizing particles. This S/N does not include the effects of the gain nonuniformity.

Minimum Ionization Response. The response to minimum ionizing particles was obtained using the K and L conversion electrons of ^{207}Bi having energies of 975.6 keV and 1048.1 keV respectively. A 1500 μ surface barrier (SB) detector was mounted behind the detector under study and served as a trigger. The maximum energy spread in the beam after having passed through the detector under study was less than 30 keV. Approximately 90 keV was lost from the beam in passing the detector under study. A differential discriminator was set to accept these two lines (which were resolved) and was used to gate the passing detector signal. In order to calibrate the system, the response of a 250 μ thick SB detector was measured. Approximately 90 keV was deposited by the 1 MeV electron beam in passing the SB detector. The response of the SB detector is seen in Fig. 7. In the same figure we show the response of the ESAD to the electron beam. In this case the most probable energy loss was 12.6 keV and the gain of the shaping amplifier was reduced by 3 for purposes of comparison. The gain realized in the avalanche zone was 21. The low channel portion of the spectrum reflects an artifically high noise content in as much as triggers associated with electrons passing the guard ring and outside the detector geometry were accepted. No collimation was used on the electron beam. The main limitation in the resolution of this spectrum is due to nonuniformity in gain. From this spectrum and Eq. 4 we infer a nonuniformity in the areal density of ionized impurities in the first epitaxial layer of 0.2%.

Noise. An analysis of the noise spectrum as a function of gain for the ESAD allows an upper limit to the dark current flowing into the avalanche zone. For this detector the current was less than 10^{-11} ampere/mm^2. Such a low current reflects on the high quality of the epitaxial material.

It should also be pointed out that the low resistivity of the epitaxial material allows the possibility of the full utilization of the high gain bandwidth product (> 100 GHz). Dielectric relaxation is not a limiting time constant.

ESSB - Epitaxial Silicon Schottky Barrier Detector

This type of detector was first introduced by J. P. Ponpon, P. Siffert, and F. Vazeille.[1] Additional properties of the design are discussed in the thesis of M. Tetefort[2] and the works of Maggiore, et al.[15] The basic

design of the detector is seen in Fig. 8. The thin silicon film is produced using a selective (impurity density dependent) etch technique developed by R. L. Meek.[6] Because of the selectivity of the etch, the uniformity of the thin film is determined by the epitaxial growth process (10% across a 2-in. diameter wafer).

Figure 9 shows the response to oxygen ions of a 4-μm thick detector fabricated using this technique.

One particularly important feature of such thin detectors when used to detect densely ionizing particles is associated with the high field in the space charge. This field can be particularly high at the edges of the depletion region and in some cases can be the cause of either charge injection and/or avalanche.[16] This gives rise to an amplification of the signal. The amplification is most likely to be not uniform. A discussion of this problem is given in the paper of Maggiore, et al,[15] where solutions are proposed for surmounting this problem.

ESD - Epitaxial Silicon Diode

This particular device was designed to be an economical, large area, long radiation lifetime, fission fragment or heavy ion detector. In addition to these features, the design was seen to have an interesting charge transport. Figure 10 shows the design. The main feature is the stacking of the p and n-type epitaxial layers to give a junction which is approximately 14 μm below the front contact. The total junction area used was 7 cm . The use of such a large area of epitaxial material again reflects on the quality of the available material. The use of the lower resistivity material was expected to give rise to a longer radiation lifetime. This particular design has successfully been thinned (substrate removed) over entire junction area using the selective etch technique of Meek.[6]

Figure 11 shows the response of the detector to a beam of 52.5-MeV oxygen ions. The scattered beam was collimated to an area of 1.8 cm^2. The resolution of the detector was limited by kinematics. The electronic contribution to the resolution as measured by the pulser was due to the Nyquist noise and the large capacitance of the detector. It is important to note the very few counts in the tail of the peak. The small shelf on the lower side of the oxygen peak is thought to be due to channeling and/or slit scattering.

Figure 12 shows the response of the detector to fission fragments.

In the course of the experiment it was observed that the charge collection efficiency had an unusual bias dependence. More charge was collected at lower biases. In addition to this fact, for oxygen ions it was also observed that for small depletion widths there was little, if any, window in the detection of alpha particles (5.4 MeV). This prompted a more complete investigation of the charge collection efficiency. The effects were reproducible even when the parameters of the detector equivalent circuit were changed and/or the filter time constants. Thus the effect was not believed to be an artifact of the electronics measurement apparatus.

Figure 13 shows the efficiency as a function of the range of oxygen ions and detector bias. The main features of this data are the low efficiencies for ranges short compared to the location of the junction and the reversal of the bias dependence as the range crosses the junction.

Figure 14 shows a more detailed dependence of the efficiency in detecting 92.5-MeV sulfur ions (range ∿ 37 μm) as a function of detector bias. Data was taken for both normal incidence and an angle of 45° with respect to the plane of the junction. The 45° data were less efficient for all biases and were less dependent on the bias.

Figure 15 gives a simplified model depicting the charge transport process which accounts for all the major features of the data. Important to the model are the following assumptions:

The charge transport involves both drift and diffusion*

$$\text{holes,} \quad J_p = e p \mu_p E - e D_p \left(\frac{\partial p}{\partial x}\right) \tag{10}$$

$$\text{electrons,} \quad J_n = e n \mu_n E + e D_n \left(\frac{\partial n}{\partial x}\right) \tag{11}$$

the field depends upon the space charge

$$\frac{\varepsilon}{e}\left(\frac{\partial E}{\partial X}\right) = (p-p_o) - (n-n_o) \tag{12}$$

the continuity equations

$$\frac{\partial p}{\partial t} = -\frac{p-p_o}{\tau_p} - \frac{1}{e}\frac{\partial J_p}{\partial X}$$

$$\frac{\partial n}{\partial t} = -\frac{n-n_o}{\tau_n} + \frac{1}{e}\frac{\partial J_n}{\partial X} \tag{13}$$

the voltage across the detector is a constant, i.e.,

$$\int_{\text{Detector}} E(X,t)\, dx = \text{constant} \tag{14}$$

and

$$J(t) = J_p(x,t) + J_n(x,t) + \frac{\varepsilon \partial E(x,t)}{\partial T} \tag{15}$$

the sum of true currents and displacement current is independent of position.

The charge transport occurs as follows:

1. The plasma in the depletion region polarizes such that the field across the depletion region is driven to zero.

2. This accumulation of charge at the edges of the depletion region creates a dipole field such that the net field between the poles is zero and the net field extending outward towards the contacts has an integral such that the voltage across the detector remains constant.

3. The charge transport between the poles and the contacts is dominated by drift.

4. The charge transport in between and out of the poles is dominated by diffusion across a distance given by the depletion width.

*Notation from L. P. Hunter, Handbook of Semiconductor Electronics.

The charge transport is slowest between the poles of the dipole (blocked region) and it is here where recombination is most important. The wider the depletion region (a longer diffusion transport) the greater the probability for recombination and inefficiency.

A simplified calculation gives the following expression for the charge collection efficiency (keeping in mind that the measurement involves an integral of image currents):

$$\xi(V) = 0.75 - \frac{0.5\ W(V)}{R} + \left(0.25 + \frac{0.5\ W(V)}{R}\right) \exp(-3\tau_p(V)/\tau_R) \qquad (16)$$

where the depletion width, W, is given by $W = 3.67\ V^{1/2} \times 10^{-4}$ cm

R is the range of the particle

and $R >> W$

the diffusion time, τ_D

$$\tau_D = \frac{W^2}{2D} = 3.36 \times 10^{-9}\ V\ (\text{volts})\ \text{sec}$$

and τ_R is the recombination lifetime.

The gross features of the data in Fig. 14 are fitted, assuming only a recombination lifetime of 2.0×10^{-6} sec. The 45° data of Fig. 4 are accounted for by simply assuming the particle is off the edge of the dipole field. One then has a portion of the transport with efficiencies as though the range were short and portions as though the range were long compared to the junction depth (see Fig. 12). These two portions have voltage dependencies which tend to cancel.

This model accounts for the features in Fig. 13 as follows: For the data having ranges long compared to the junction depth, the inefficiency is determined by the charge lost in storage in the blocked-dipole region, and therefore is least for the smallest depletion width. For the data having ranges short compared to the junction depth, the efficiency is determined by the overlap of the depletion width with the plasma and therefore is greatest for the widest depletion widths.

IV. FUTURE PROSPECTS

Epitaxial silicon, because it can be made thin, with low resistivity and with internal amplification, will offer the following possible important advantages over other types of detectors:

1. Small multiple scattering,
2. High spacial resolution,
3. Short response time,
4. Improved particle/heavy ion identification,
5. Improved signal-to-noise in energy and fast timing measurements, and
6. Longer irradiation lifetime.

ACKNOWLEDGEMENTS

The author gratefully acknowledges stimulating conversations with Drs. B. Hyams, CERN, R. Fair, BTL, V. Radeka, BNL, C. Maggiore, P. Goldstone, N. Jarmie, S. Depp, P. W. Keaton, J. Narud, LASL. The author thanks P. Kelley for the typing of this manuscript.

REFERENCES

1. J. P. Ponpon, P. Siffert, and F. Vazeille, Thin dE/dX Detectors of Uniform Thickness Made on Epitaxial Silicon, Nucl. Instr. and Meth. 112, 465-467, September 1973.
2. A. Tetefort, Etude D'un Nonveau Procede de Preparation de Detecteurs Nucleaires dE/dX Minces, These A L'Universite de Clermont-Ferrand, France, 100 pages, Janvier 1976.
3. C. R. Gruhn, A Thin All Epitaxial Silicon Detector with Internal Amplification, IEEE Trans. Nucl. Sci. NS-23, 145-152, February 1976.
4. C. R. Gruhn, S. Depp, Nelson Jarmie, and P. W. Keaton, Nonlinear Aspects of the Avalanche Gain Mechanism in Silicon Avalanche Diodes, Nucl. Instr. and Meth. (to be published).
5. C. R. Gruhn, P. D. Goldstone, and Nelson Jarmie, An All Epitaxial Silicon Diode Heavy Ion Detector, IEEE Trans. Nucl. Sci. NS-24, February 1977 (to be published).
6. R. L. Meek, W. M. Gibson, and R. H. Braun, Preparation of Supported, Large-Area, Uniformly Thin Silicon Films for Particle-Channeling Studies, Nucl. Instr. Meth. 94, 435-442, June 1971.
7. R. L. Williams and P. Webb, Transistor Form of Nuclear Particle Detector, IRE Trans. Nucl. Sci. NS-8, 35-42, January 1961.
8. G. C. Huth, Recent Results Obtained with High Field, Internally Amplifying Semiconductor Radiation Detectors, IEEE Trans. Nucl. Sci. NS-13, 36-42, February 1966.
9. P. Webb and A. R. Jones, Large Area Reach-Through Avalanche Diodes for Radiation Monitoring, IEEE Trans. Nucl. Sci. NS-21, 151-158, February 1974.
10. P. P. Webb and R. J. McIntyre, Large Area Reach-Through Avalanche Diodes for X-Ray Spectroscopy, IEEE Trans. Nucl. Sci. NS-23, 138-144, February 1976.
11. W. T. Read, A Proposed High-Frequency Negative Resistance Diode, B.S.T.J. 37, 401-446, March 1958.
12. S. L. Miller, Avalanche Breakdown in Germanium, Phys. Rev. 99, 1234-1241, August 1955.
13. S. M. Sze, Physics of Semiconductors, Wiley 1969, page 675.
14. C. Maggiore, P. D. Goldstone, C. R. Gruhn, H. DeHaven, S. Stotlar, and Nelson Jarmie, Thin Epitaxial Silicon For dE/dX Detectors, IEEE Trans. Nucl. Sci. NS-24, February 1977.
15. F. J. Walter, Multiplication in the Fission Fragment Pulse Height Response of Silicon Surface Barriers, IEEE Trans. Nucl. Sci. NS-11, 232-237, June 1964.

FIGURE CAPTIONS

Fig. 1. Schematic design of an epitaxial silicon avalanche diode (ESAD).

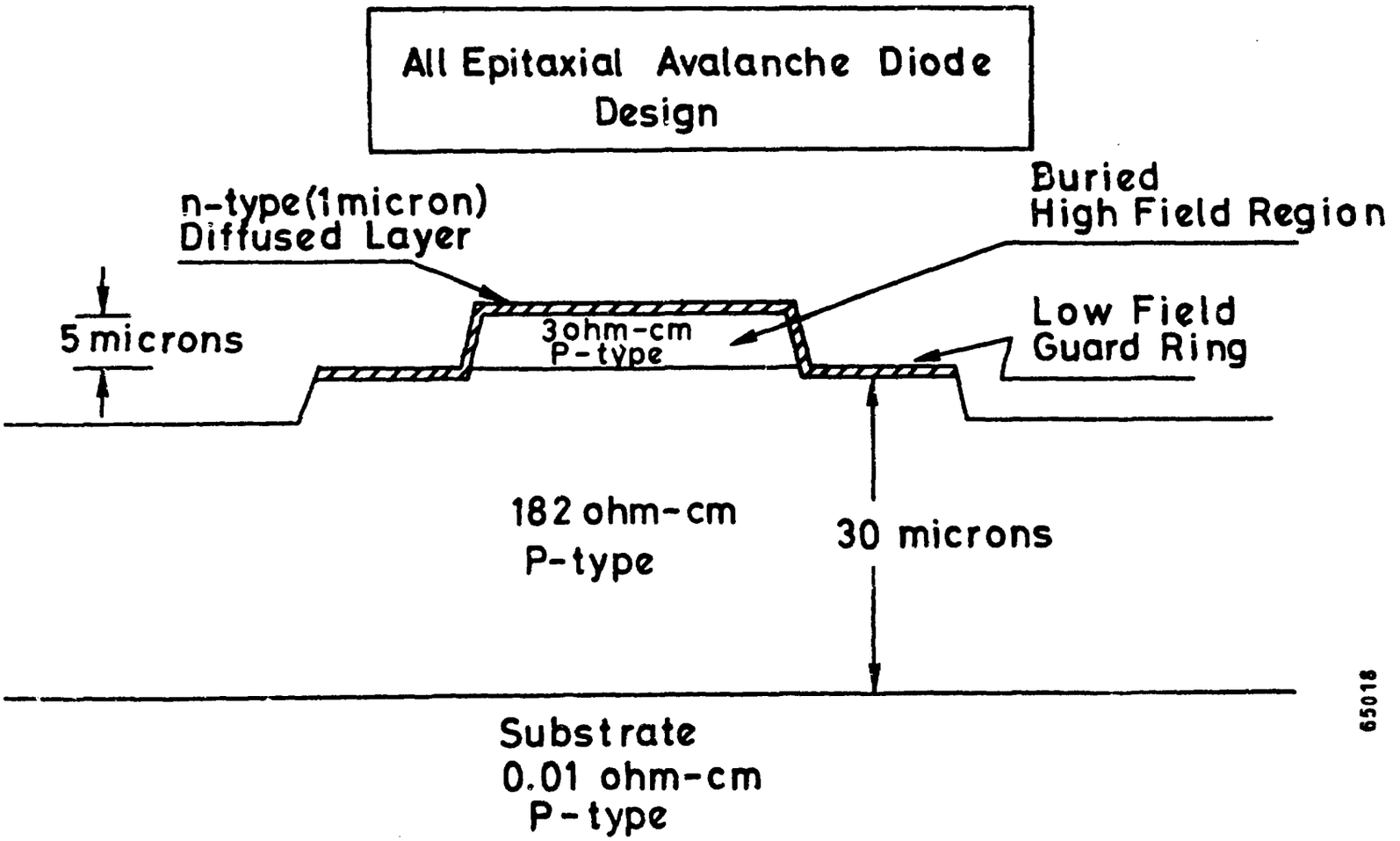

Fig. 1

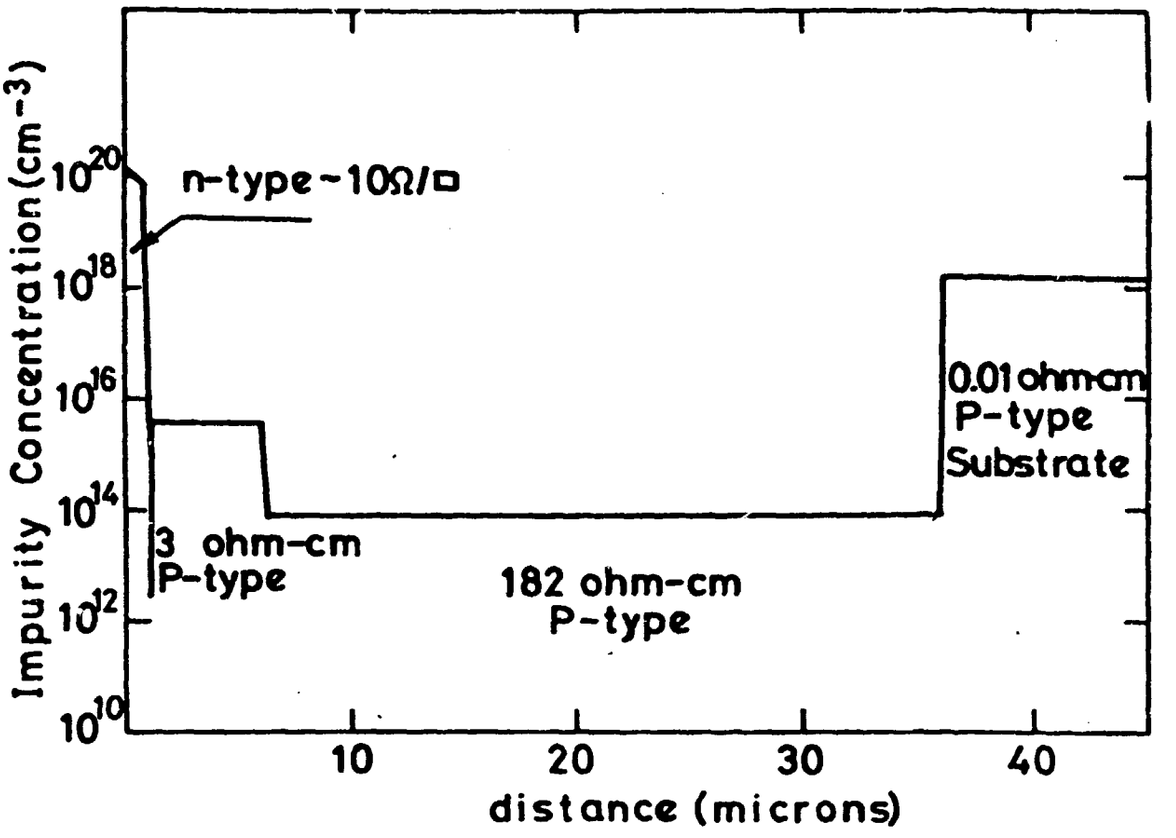
Impurity Concentration (cm⁻³)
10²⁰
10¹⁸
10¹⁶
10¹⁴
10¹²
10¹⁰
n-type ~10Ω/□
3 ohm-cm
P-type
182 ohm-cm
P-type
0.01 ohm-cm
P-type
Substrate
10
20
30
40
distance (microns)

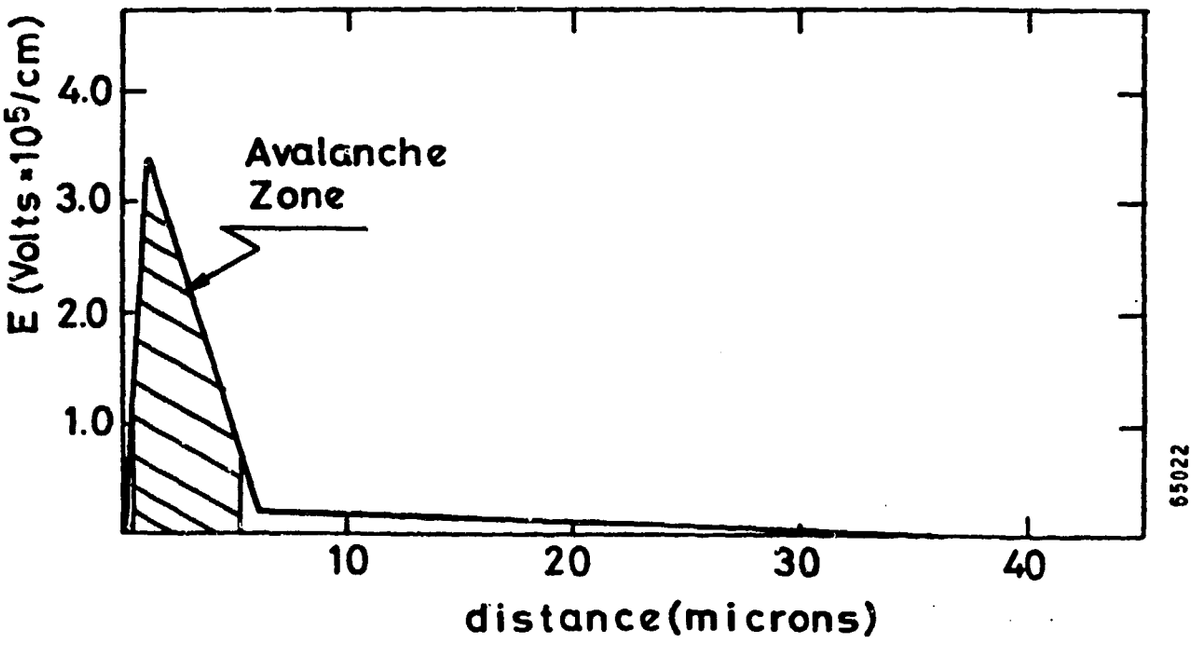
E (Volts * 10⁵/cm)
4.0
3.0
2.0
1.0
Avalanche
Zone
10
20
30
40
distance (microns)
65022

Fig. 2

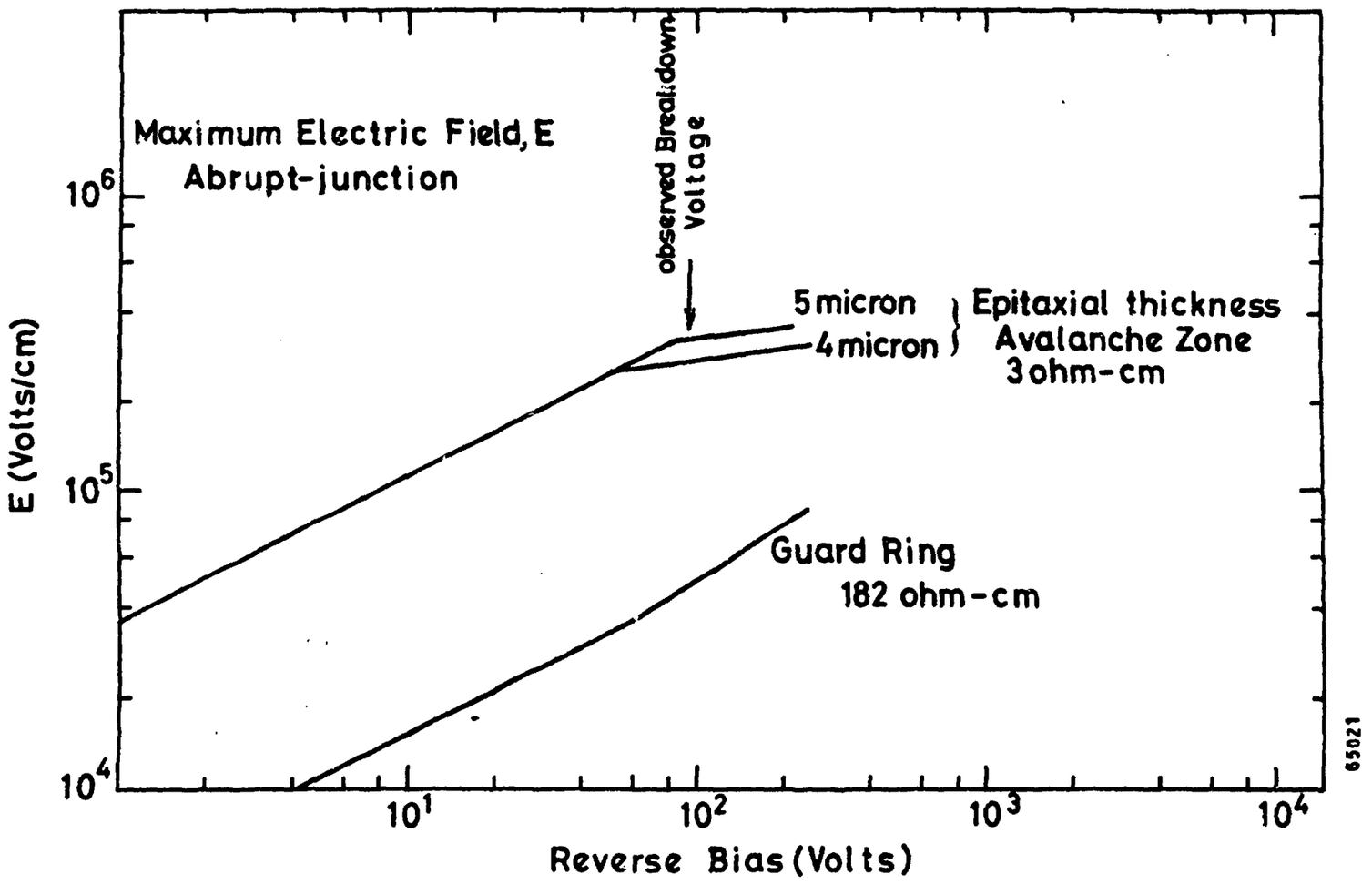
Maximum Electric Field, E
Abrupt-junction
observed Breakdown Voltage
5 micron
4 micron
Epitaxial thickness
Avalanche Zone
3 ohm-cm
Guard Ring
182 ohm-cm
E (Volts/cm)
10^6
10^5
10^4
10^1
10^2
10^3
10^4
Reverse Bias (Volts)
65021

Fig. 3

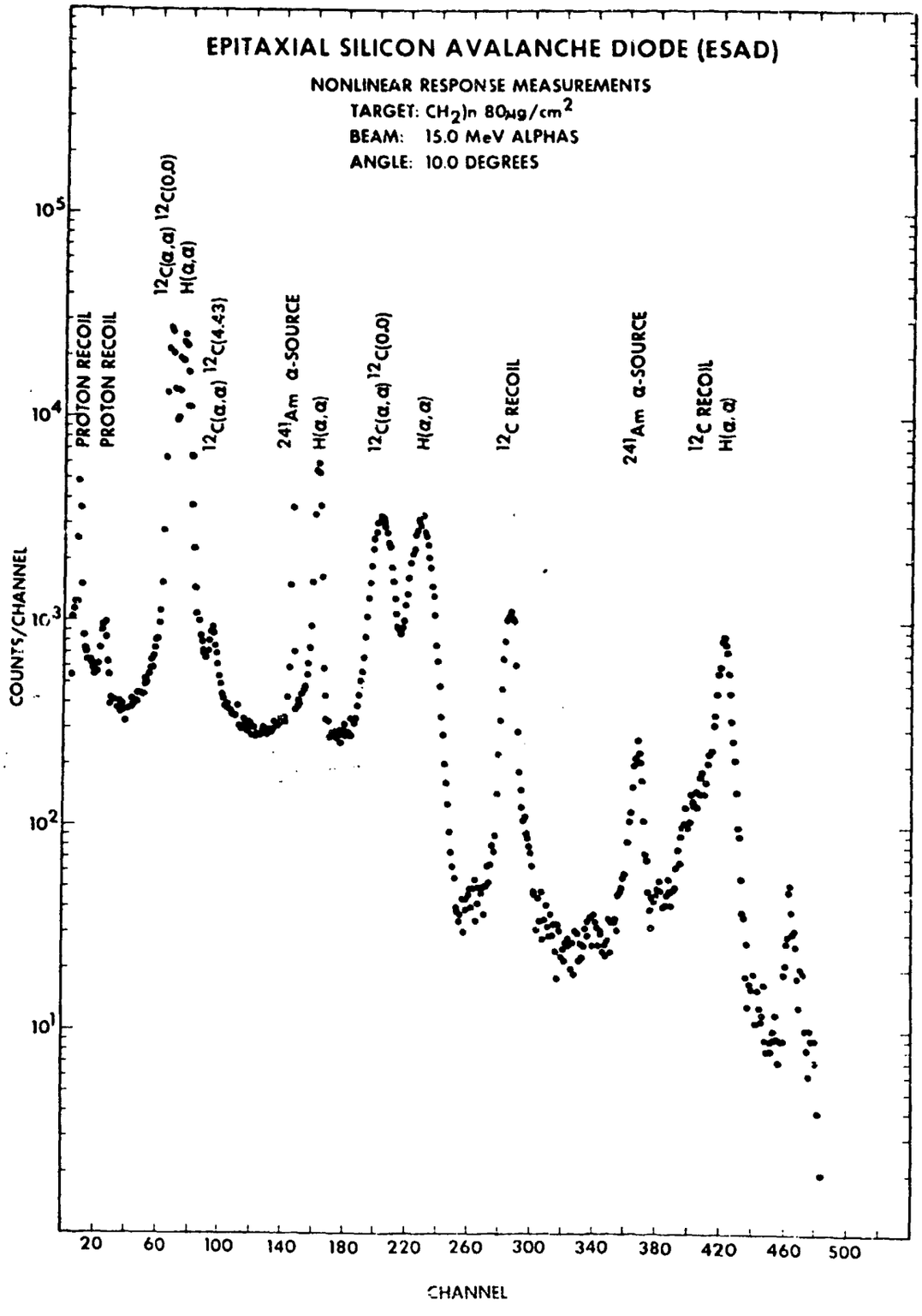
EPITAXIAL SILICON AVALANCHE DIODE (ESAD)
NONLINEAR RESPONSE MEASUREMENTS
TARGET: CH_2)n 80μg/cm^2
BEAM: 15.0 MeV ALPHAS
ANGLE: 10.0 DEGREES
COUNTS/CHANNEL
CHANNEL
PROTON RECOIL
PROTON RECOIL
$^{12}C(\alpha,\alpha)^{12}C(0.0)$
H(α,α)
$^{12}C(\alpha,\alpha)^{12}C(4.43)$
^{241}Am α-SOURCE
H(α,α)
$^{12}C(\alpha,\alpha)^{12}C(0.0)$
H(α,α)
^{12}C RECOIL
^{241}Am α-SOURCE
^{12}C RECOIL
H(α,α)

Fig. 4

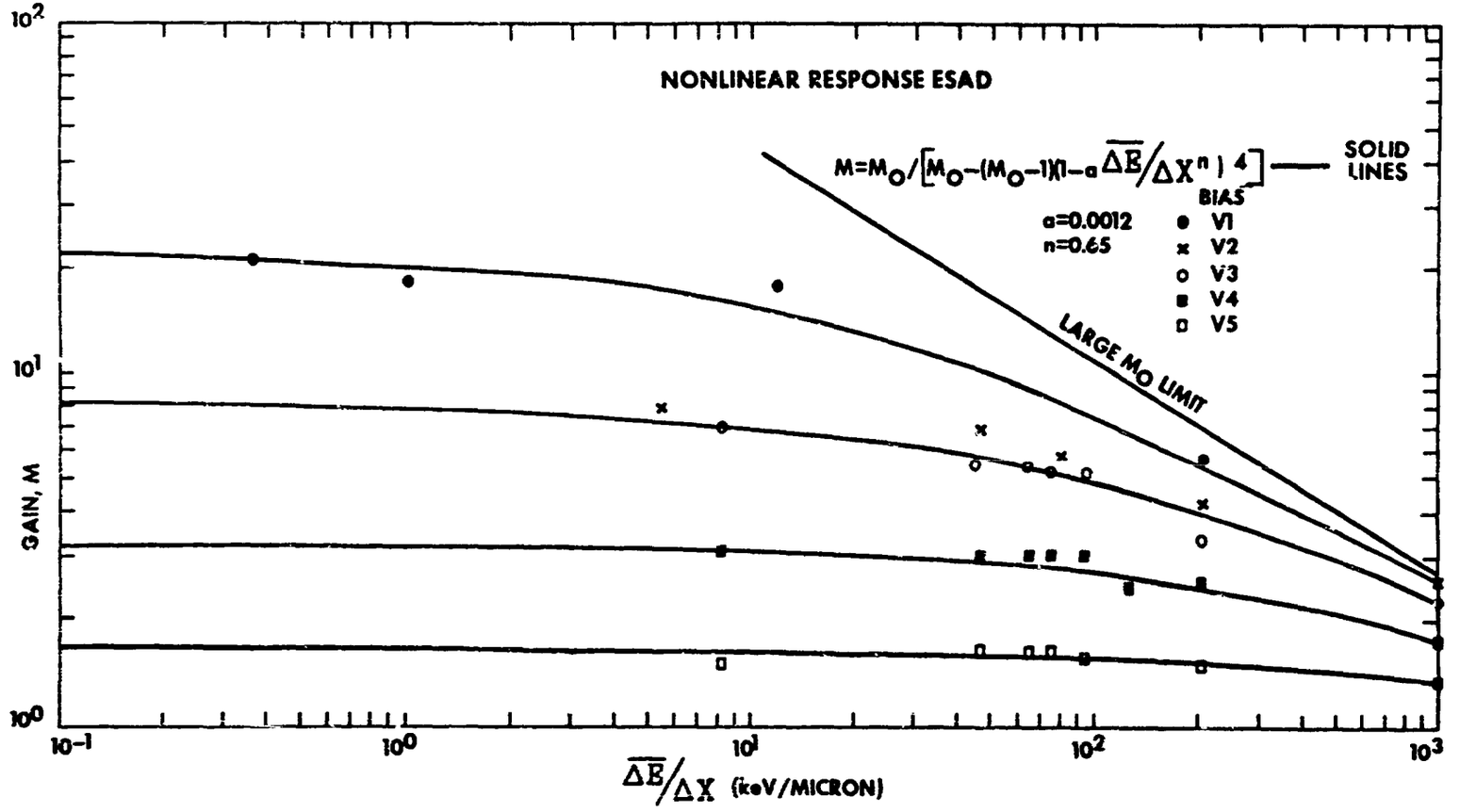

Fig. 5

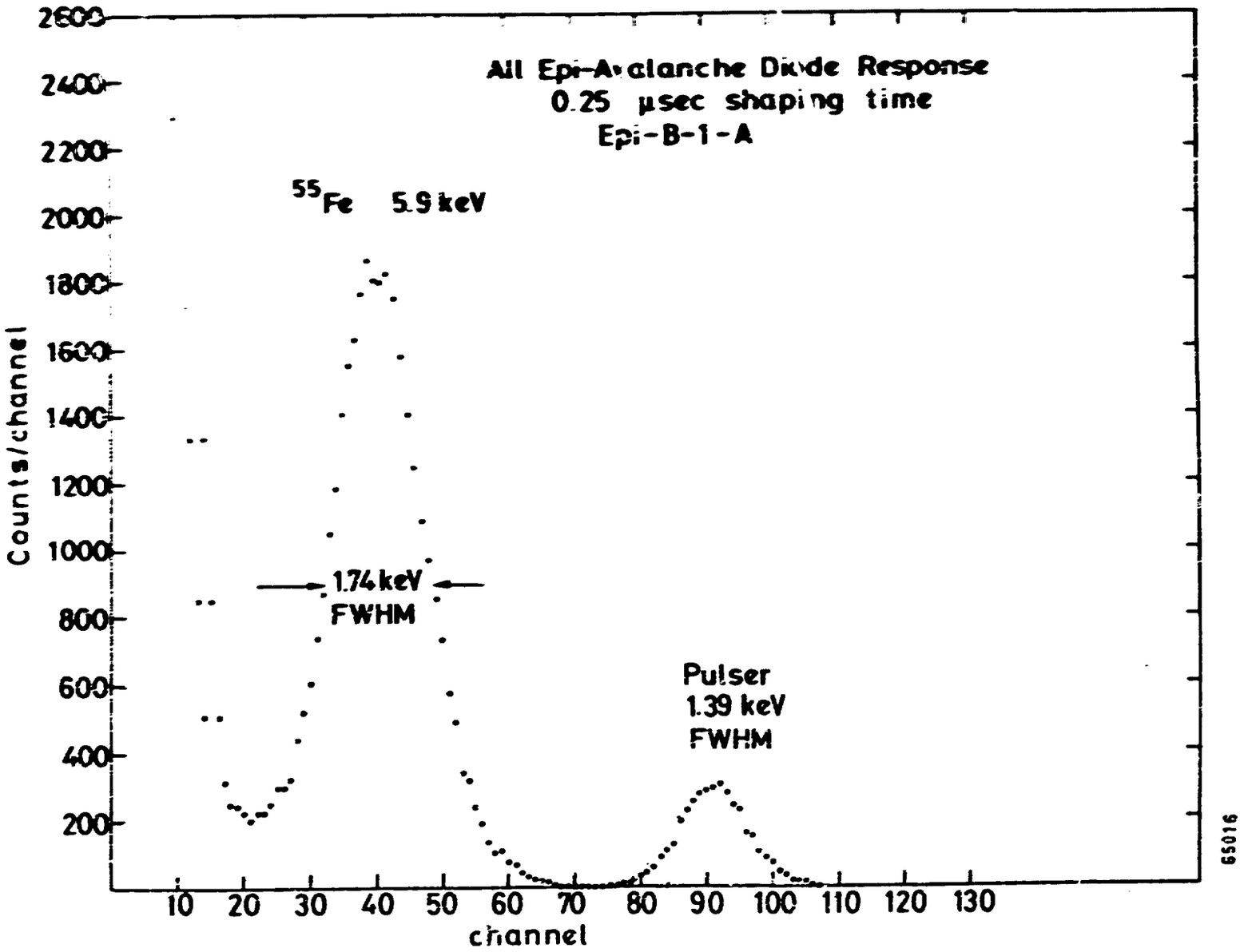
All Epi-Avalanche Diode Response
0.25 µsec shaping time
Epi-B-1-A
55Fe 5.9 keV
1.74 keV
FWHM
Pulser
1.39 keV
FWHM
Counts/channel
channel
2600
2400
2200
2000
1800
1600
1400
1200
1000
800
600
400
200
10 20 30 40 50 60 70 80 90 100 110 120 130
65016

Fig. 6

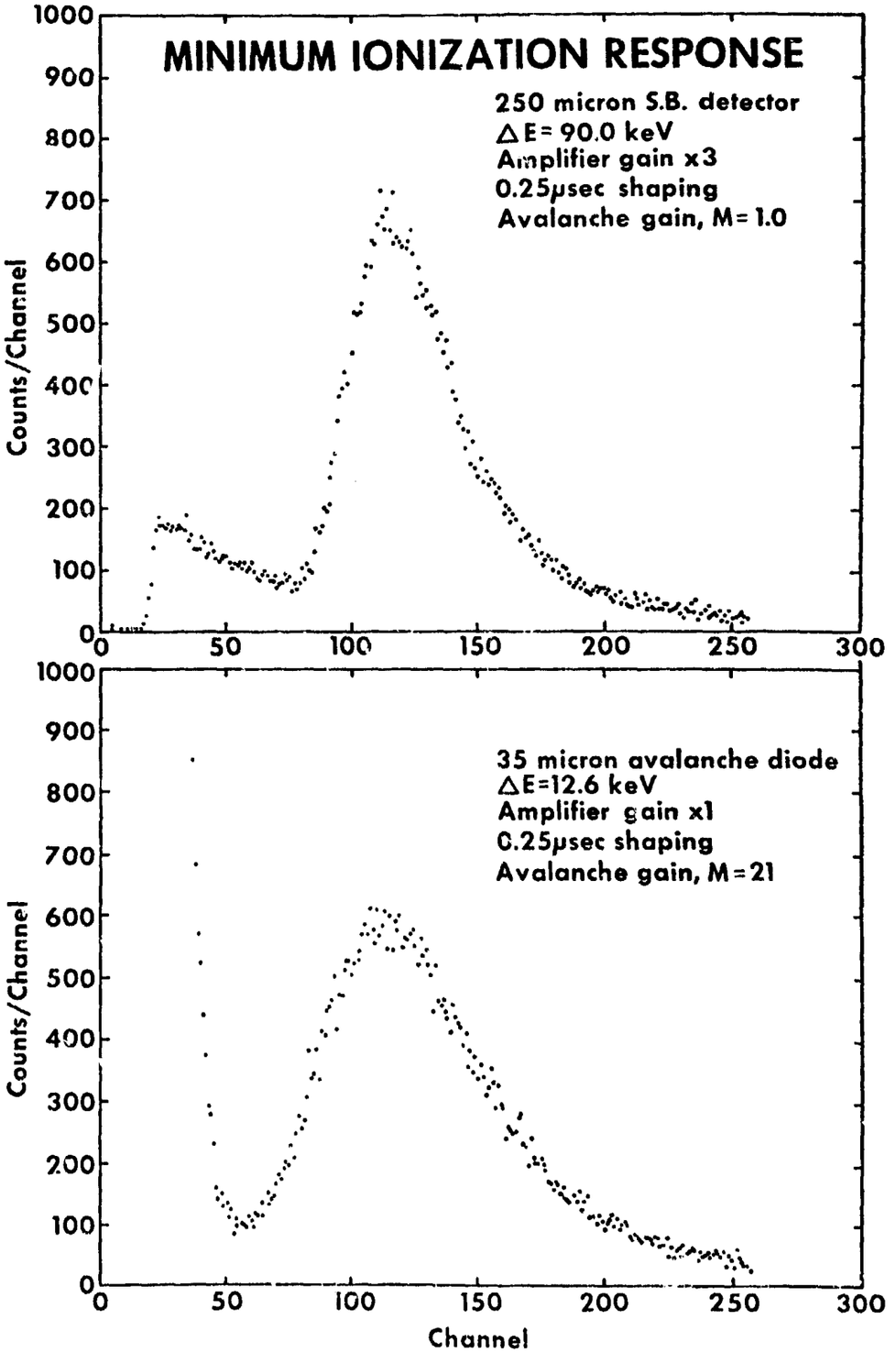

Fig. 7

EPITAXIAL SILICON SURFACE BARRIER (ESSB) DESIGN

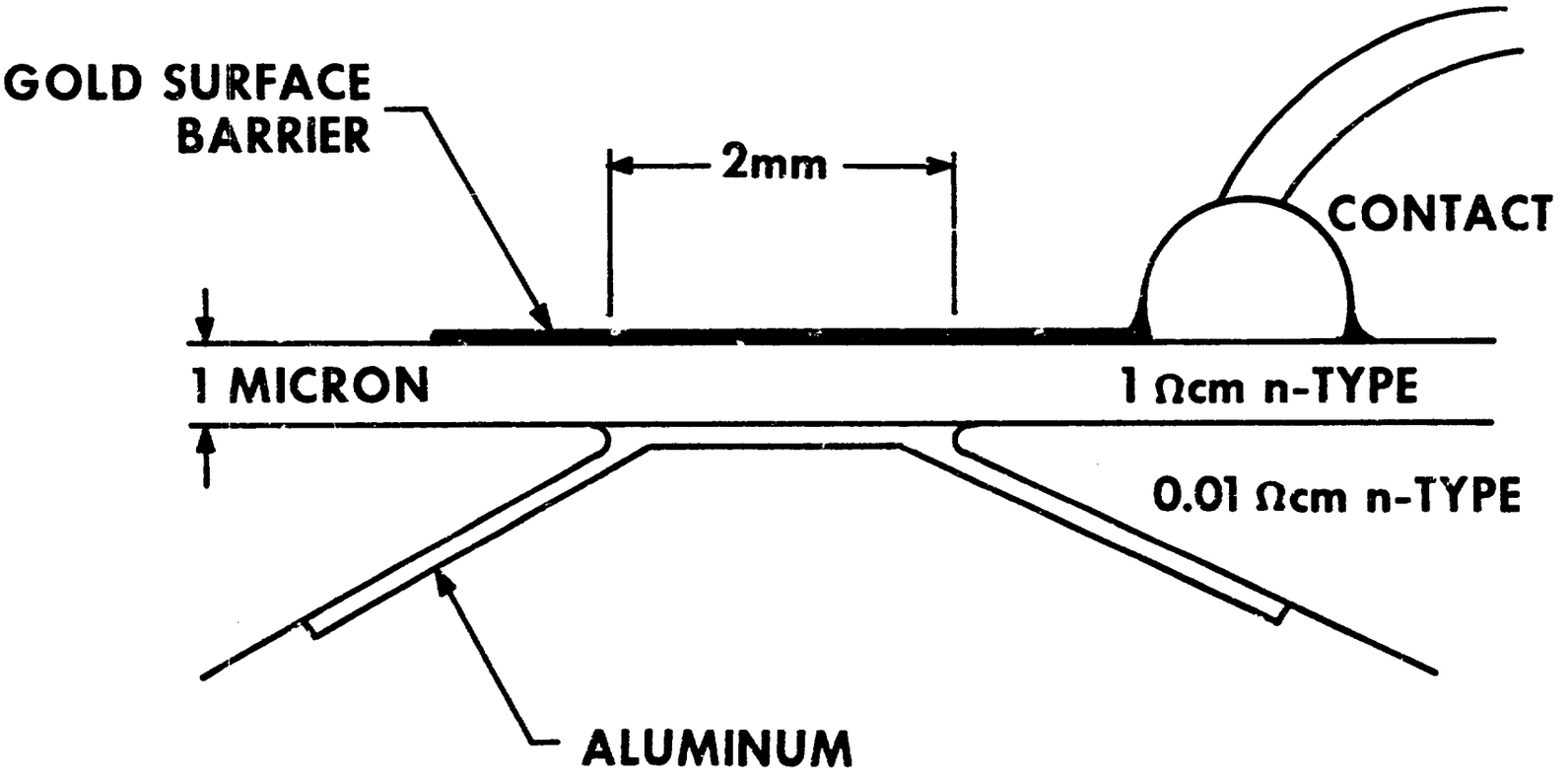

Fig. 8

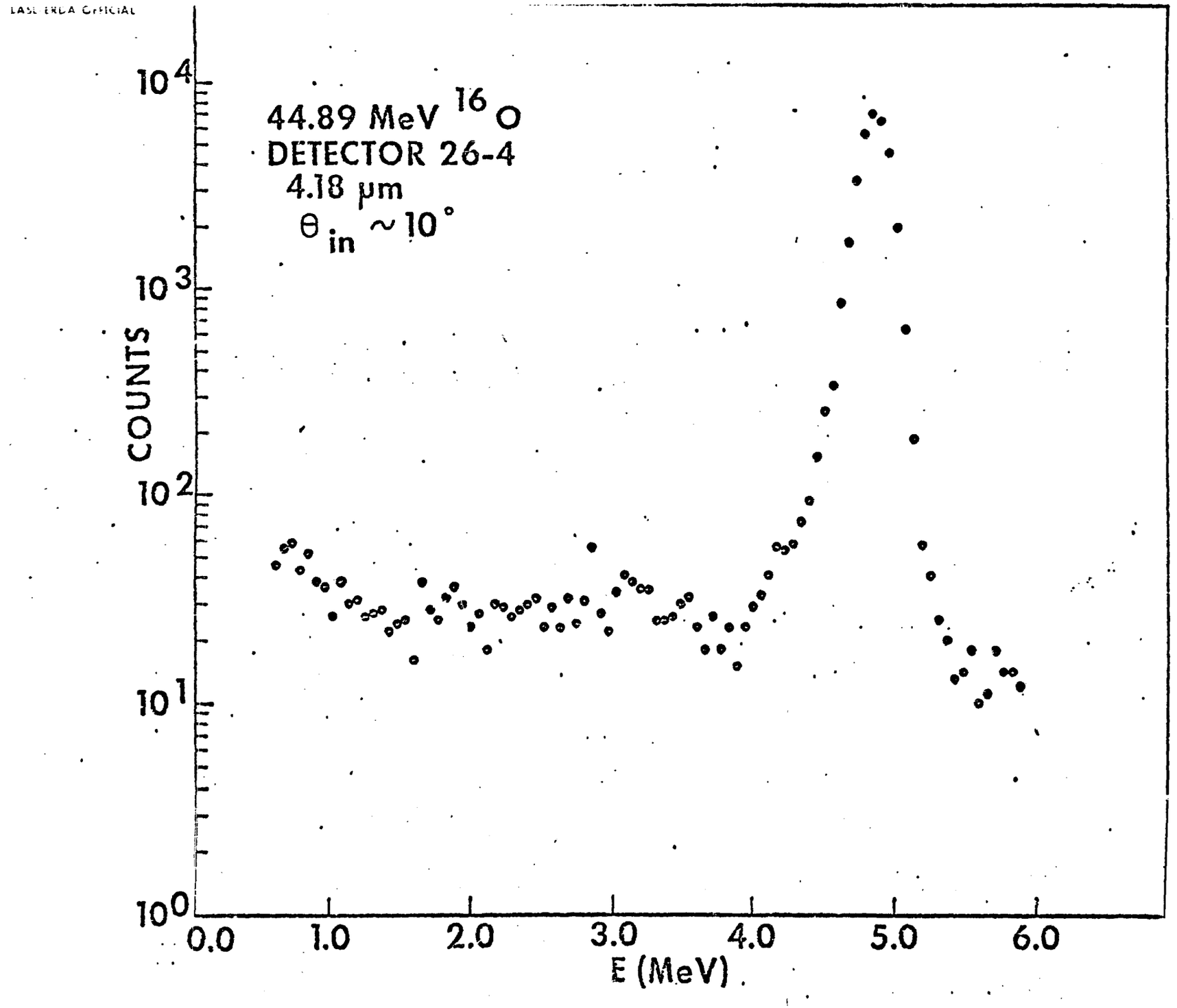

EPITAXIAL SILICON DIODE (ESD)

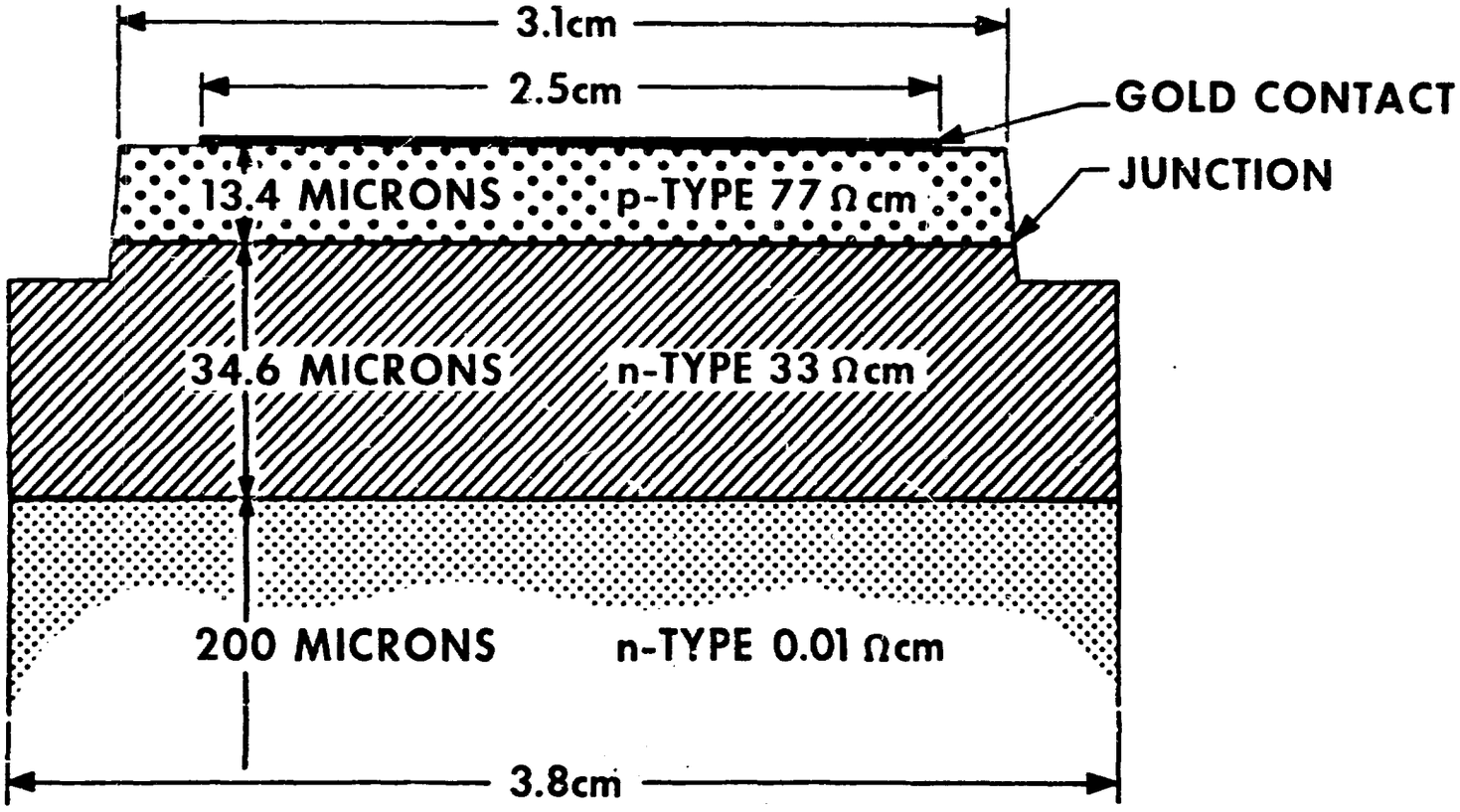

Fig. 10

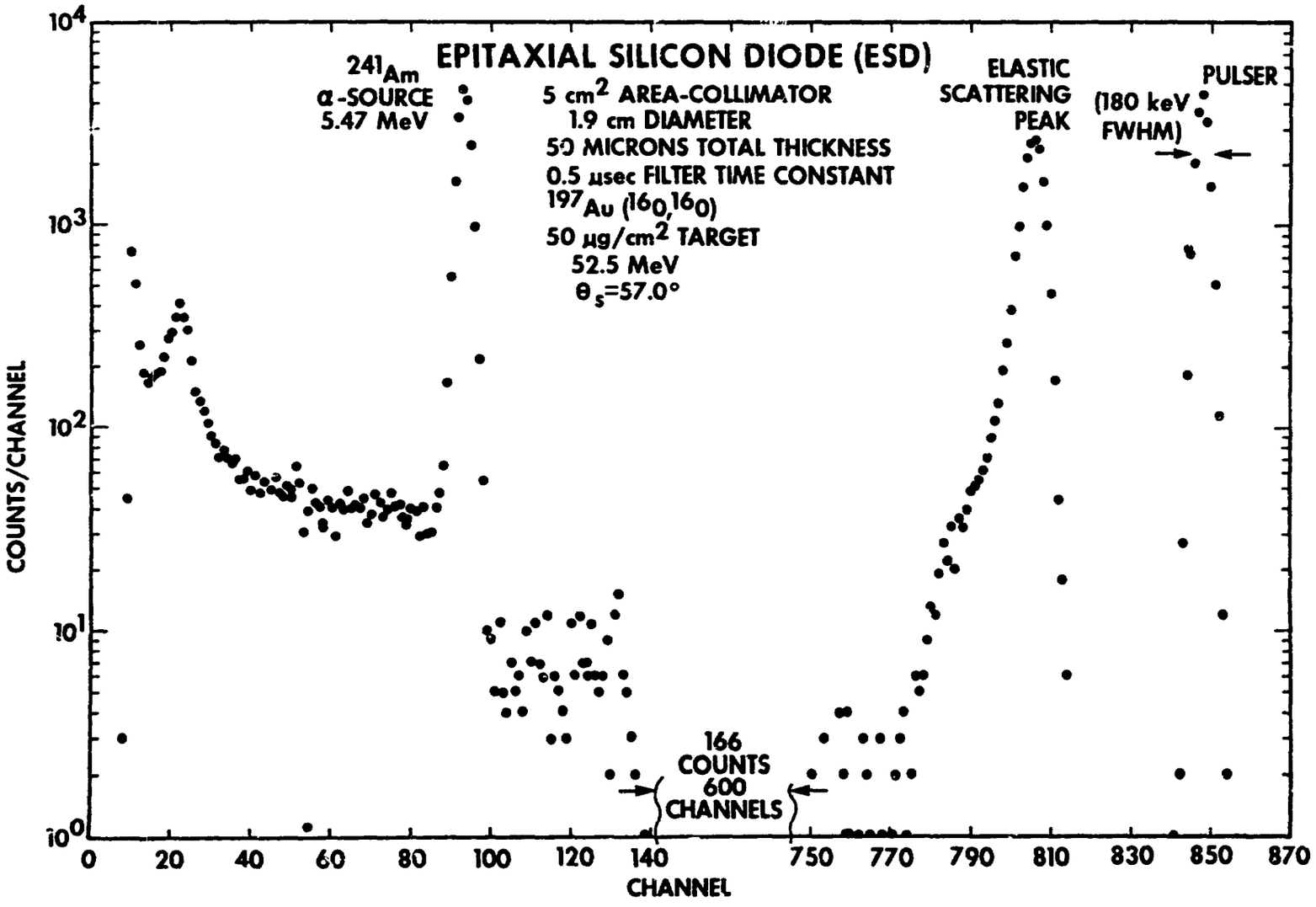

Fig. 11

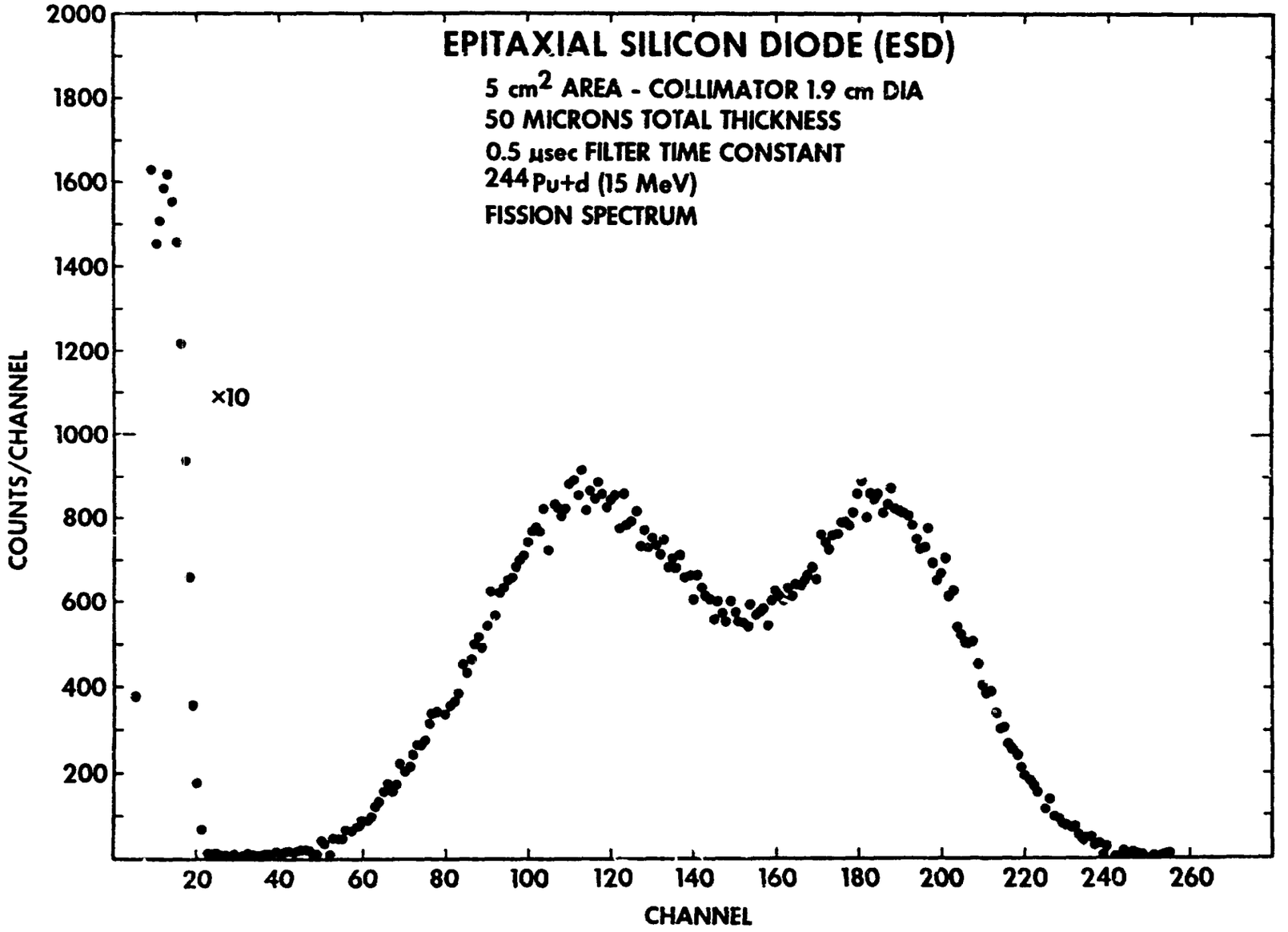
EPITAXIAL SILICON DIODE (ESD)
5 cm2 AREA - COLLIMATOR 1.9 cm DIA
50 MICRONS TOTAL THICKNESS
0.5 µsec FILTER TIME CONSTANT
244Pu+d (15 MeV)
FISSION SPECTRUM
×10
COUNTS/CHANNEL
CHANNEL
2000
1800
1600
1400
1200
1000
800
600
400
200
20
40
60
80
100
120
140
160
180
200
220
240
260

Fig. 12

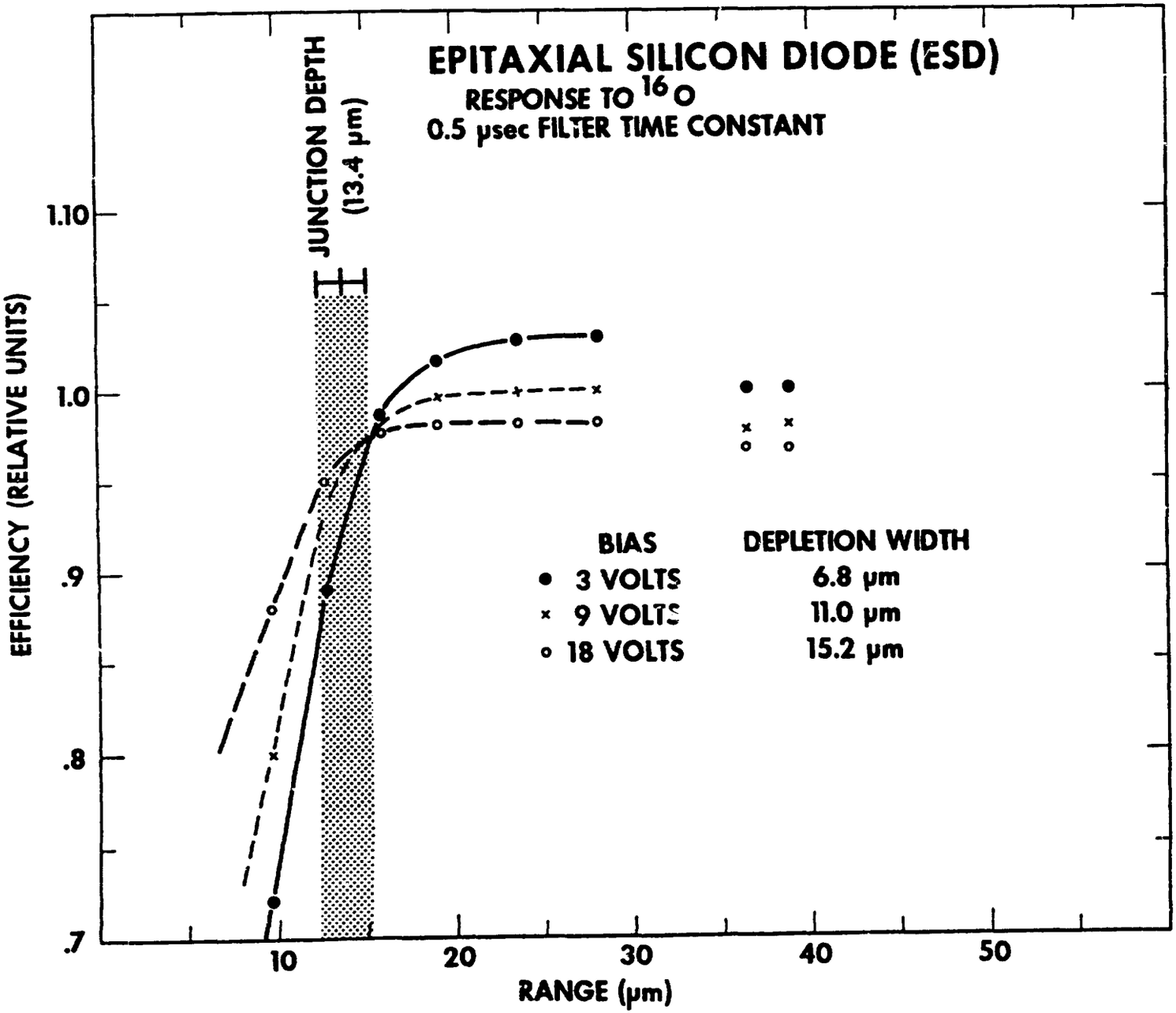
EPITAXIAL SILICON DIODE (ESD)
RESPONSE TO ^{16}O
0.5 μsec FILTER TIME CONSTANT
JUNCTION DEPTH
(13.4 μm)
EFFICIENCY (RELATIVE UNITS)
1.10
1.0
.9
.8
.7
10
20
30
40
50
RANGE (μm)
BIAS
DEPLETION WIDTH
● 3 VOLTS
6.8 μm
× 9 VOLTS
11.0 μm
○ 18 VOLTS
15.2 μm

Fig. 13

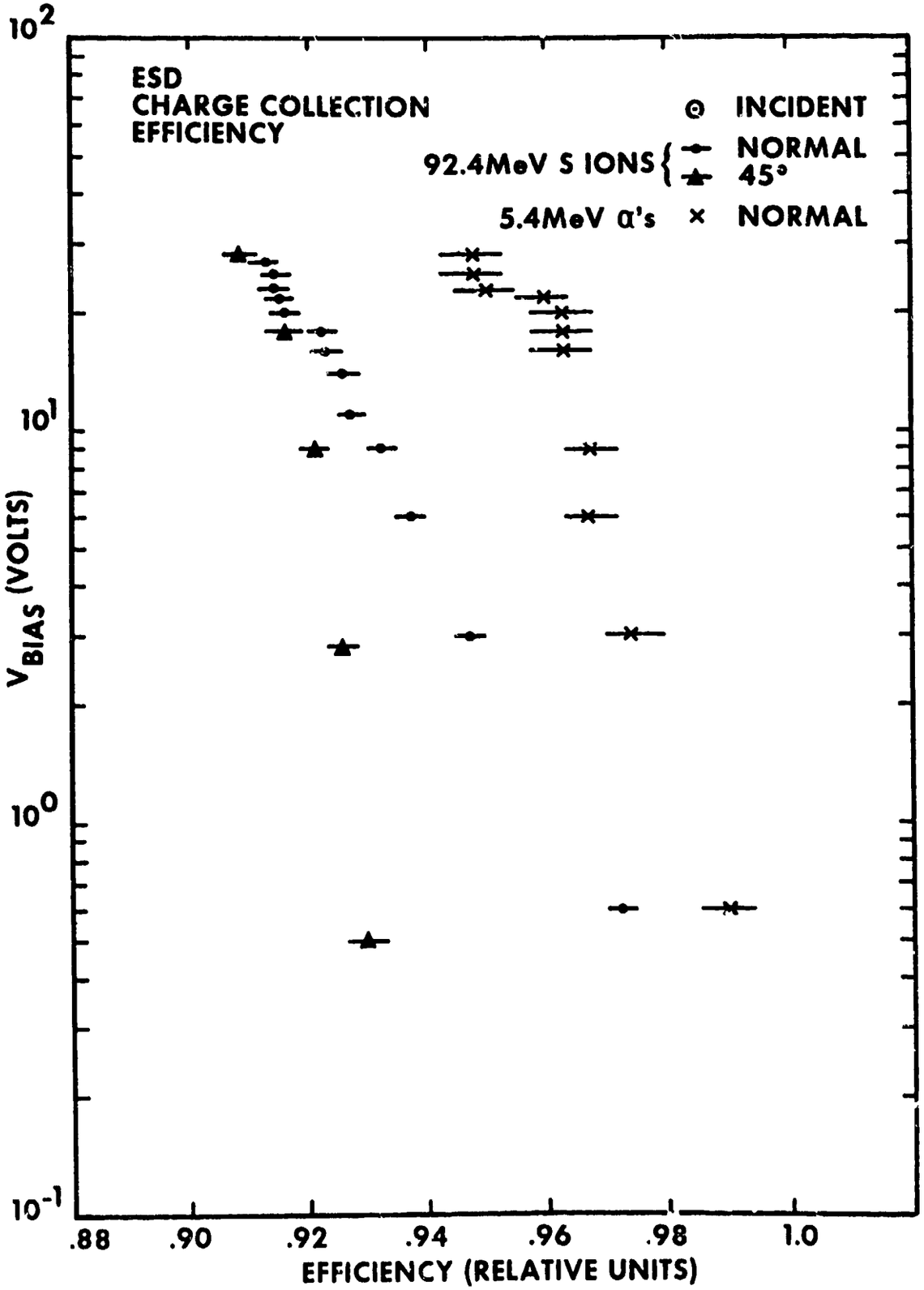
ESD
CHARGE COLLECTION
EFFICIENCY
INCIDENT
92.4MeV S IONS
NORMAL
45°
5.4MeV α's
NORMAL
10^2
10^1
10^0
10^{-1}
V_{BIAS} (VOLTS)
.88
.90
.92
.94
.96
.98
1.0
EFFICIENCY (RELATIVE UNITS)

Fig. 14

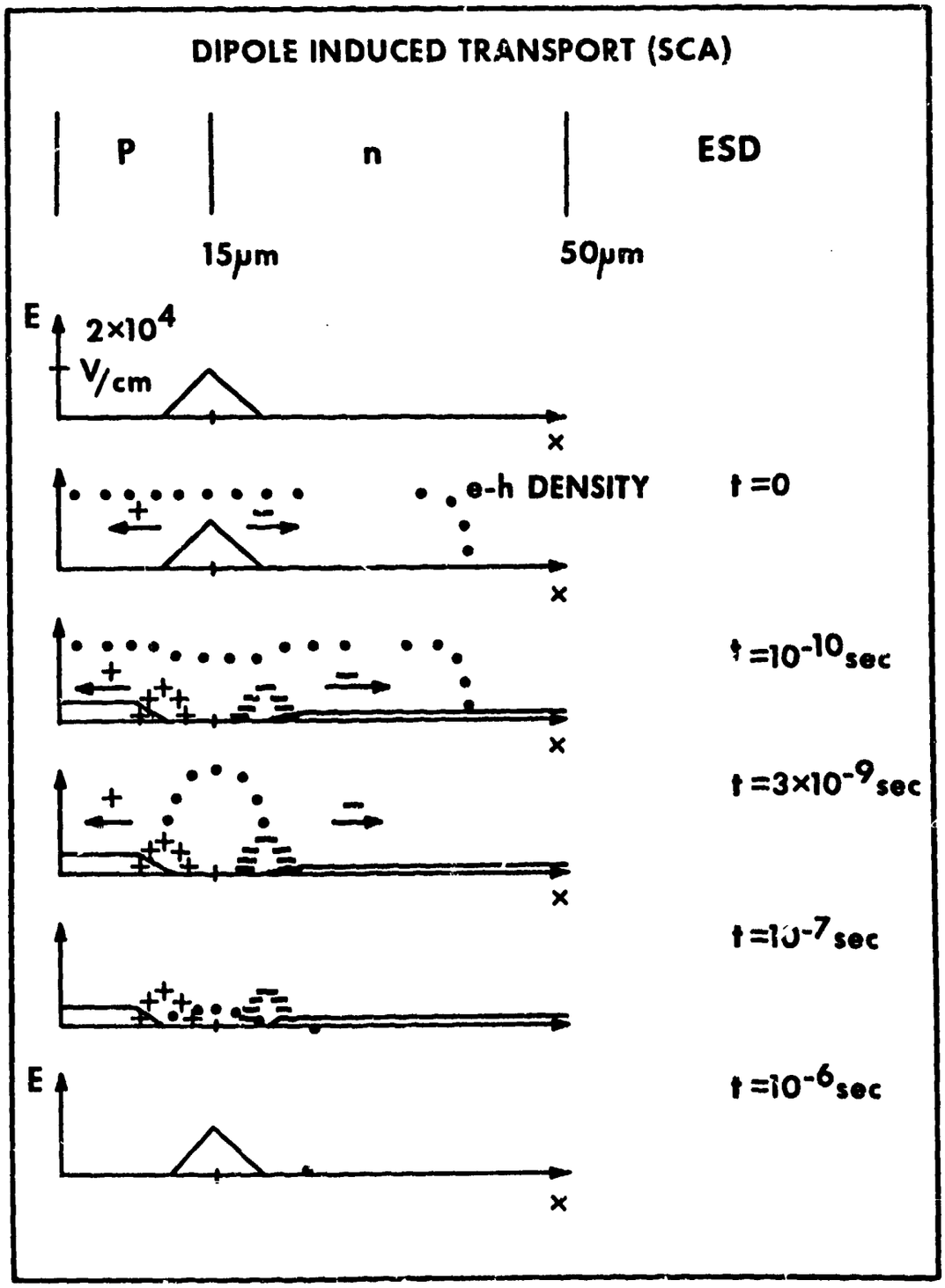
DIPOLE INDUCED TRANSPORT (SCA)
P
n
ESD
15μm
50μm
E
2×10^4
V/cm
x
e-h DENSITY
t =0
t =10^-10 sec
t =3×10^-9 sec
t =10^-7 sec
E
t =10^-6 sec
x

Fig. 15